AIAA JOURNAL
Vol. 46, No. 6, June 2008

Impedance Boundary Condition for Truncated Open Spaces

K.-Y. Fung,* X. D. Jing,† Z. B. Lu,‡ and T. Wang§
Hong Kong Polytechnic University,
Hong Kong, People's Republic of China

DOI: 10.2514/1.31925

The propagation of waves governed by hyperbolic systems at a surface is in general reflective. The numerical solution of many problems in mechanics necessitates the truncation of an open space to a finite domain. The reflectivity of the boundary of a truncated domain can be effectively characterized by a few parameters and implemented as a time-domain impedance boundary condition. It is shown that the concept of a time-domain impedance boundary condition affords a simple and effective treatment of waves, allowing them to exit the surfaces of a truncated domain as a causal, local, space–time continuation rather than a global boundary confinement. We present and discuss the open-space impedances of radiative and convective fields, their modeling, analytic structures, implementation, and solution effectiveness as an open-space impedance boundary condition. We further propose a general methodology for numerical definition of open-space impedance and its application within existing schemes to reduce truncated domains and computational resources.

Nomenclature

c	=	sound speed
$\cos\zeta$	=	$\vec{n}\cdot\boldsymbol{j}$
$\cos\xi$	=	$\vec{n}\cdot\boldsymbol{i}$
g	=	finite-width convection-effect coefficient
$\boldsymbol{i}, \boldsymbol{j}$	=	Cartesian basis vectors
j	=	$\sqrt{-1}$ complex constant
k	=	wave number
L	=	operator of the governing equation
M	=	Mach number
$\vec{n}$	=	surface normal vector
r	=	$\sqrt{x^2+y^2}$ radial distance
s	=	$j\omega$ Laplace variable
t, T	=	time measure, time period
U	=	freestream speed
u, u_r, q	=	horizontal, radial, and magnitude of the velocity components
$W(t)$	=	reflection impulse
$\hat{W}(\omega)$	=	reflection coefficient
$Z(\omega)$	=	impedance
α	=	$\sqrt{1-M^2\sin^2\theta}$
β	=	$\sqrt{1-M^2}$
Δt	=	time step
θ	=	angular orientation
ϑ	=	$\cos\theta\cos\xi+\beta^2\sin\theta\cos\zeta$
ρ	=	velocity ratio
ρ_0	=	density
Γ	=	domain bounding surface
ϕ, ψ	=	wave solutions
ω	=	angular frequency
$\wedge$	=	arête, Fourier-transform quantifier

Presented as Paper 2870 at the 10th AIAA/CEAS Aeroacoustics Conference, Manchester, England, U.K., 10–12 May 2004; received 7 May 2007; accepted for publication 1 February 2008.

*Professor, Department of Mechanical Engineering, Associate Fellow AIAA.

†Research Associate, Department of Mechanical Engineering; currently Beijing University of Aeronautics and Astronautics; jingxd@buaa.edu.cn.

‡Research Assistant, Department of Mechanical Engineering.

§Research Associate, Department of Mechanical Engineering; currently School of Mechanical Engineering, Shanghai Jiao Tong University; twang@sjtu.edu.cn.

I. Introduction

NUMEROUS problems in mechanics involve time-progressing solutions for open infinite spaces, but the domain in which these problems are discretized (by, for example, finite-difference/element methods for solutions of equation models on the digital computer) must be of finite numerical (and hence physical) dimensions. The truncation of an infinite space to a finite space immediately raises the following questions:

1) What is a suitable size?

2) What conditions are to be imposed on the solution variables at the boundaries of the truncated domain?

3) How can these conditions be incorporated into the solution process accurately and efficiently?

Various methods such as the artificial boundary condition or nonreflecting boundary condition have been proposed for imposing constraints on the solution variables at the boundary Γ of a truncated domain. The objective of these methods is to allow the solution being advanced on the truncated domain to evolve as it would if advanced on a larger or unbounded infinite domain. These methods find applications in a wide range of equation models, from the Navier–Stokes equations in fluid mechanics to the Maxwell equations in electromagnetism. A common feature in these equation models is the Laplacian operator ∇^2 that renders them spatially elliptic and requires their solution be bounded in all directions. The importance and level of difficulty of this topic have been summarized in two major review papers by Givoli [1] and Tsynkov [2]. Both authors categorized the majority of methods for posing boundary conditions of truncated domains into local and nonlocal/global methods, commented on the inadequacies of the local methods, and advocated various approaches to imposing integral/global constraint on the dependent variables and their normal derivatives on a surface Γ separating the truncated domain and its exterior of infinite extent. No significant approach has since been found to reassess Tsynkov's remark [2] that "the construction of the ideal boundary conditions. . .remains a fairly remote possibility" and Roe's remark cited in Govoli [1] that "A recurring frustration in computational fluid dynamics is the apparent difficulty of giving numerical expression to very simple statements. . .that the boundary is transparent to waves of any kind." There is, however, a separate class of methods that circumvent the closure problem of the Laplacian operator by patching a layer of wave-absorbing solution model and grid to the truncated domain to provide a buffer to the numerically truncated solution (see, for example, Hu [3]).

The developments of the artificial and nonreflecting boundary conditions for the closure of a solution on a numerically truncated domain were based on two principal assumptions. The first is that the solution progresses locally as waves propagating across Γ, and the second is that the constraints on the solution at Γ are consistent with the requirement that the solution remains bounded at infinity. The progression of the solution as waves provides a theoretical basis for the development of local methods as a set of Cauchy initial data (i.e., the values of a function and its normal derivative on a noncharacteristic contour of finite spatial and temporal extents by the method of characteristics), but it is hampered by the notorious difficulty of consistently, efficiently, and accurately extending the Cauchy data on Γ elsewhere as a solution in more than one spatial dimension. Nonetheless, many local methods imposing algebraic/differential constraints on the Cauchy values at Γ have been proposed (e.g., [4]). The second assumption, known as the Sommerfeld radiation condition in classical mechanics, is required as a result of having to solve the Fourier-transformed wave equation (the Helmholtz equation) as an elliptic system on an infinite domain. This assumption has led to developments of local constraints as a set of asymptotically decaying wave modes applicable to boundaries of sufficiently large domains [5], sequences of local constraints for progressively better compliance of the assumption [6], nonlocal constraints as solutions to analytically equivalent easily solvable auxiliary problems [2], or localized global constraints [7] as approximations to the Kirchhoff–Helmholtz integral on Γ (see [2]).

Both assumptions are germane to the solution of steady-state boundary-value problems, which are often achieved through an iterative process equivalent to the propagation of error waves (nonuniformity unsupported by the spatial operator) in pseudotime. An accurate numerical solution is achieved only when all errors, measured as a broad spectrum of solution residue, are allowed to escape the confinement of the numerical boundary. Unless the conditions on the artificial boundaries allowed all residue-waves to escape or to be perfectly absorbed [3], their reflections would remain somewhere within the computational domain until dissipated slowly by some physical or numerical damping mechanisms. We will see that for a nondissipative solver, letting all waves go out (and, at the same time, preventing the entrance of waves at a boundary Γ) is generally a conflictive paradigm and a formidable objective to which most researchers on this topic subscribe [1]. Furthermore, over a finite computing time, all waves would only have moved a finite distance from a finite boundary; their corresponding effect due to the elliptic operator from that distance on the solution at Γ would generally not be the same as if they had reached infinity. Strictly speaking, the second principal assumption has only theoretic relevance to the open-space solution that should not and cannot be attained numerically over finite time at a finite boundary Γ.

We propose instead to set a computationally attainable objective of defining or characterizing the boundary conditions for the solution to be computed on a truncated finite domain that corresponds to the same solution, but computed on a larger finite domain. We will examine the concept of wave reflection from its definition to the characterization of a reflective surface and show that any real or imagined surface has a specific resistance to a propagating wave and is therefore reflective, in general. We then define the impedance of an open space and show how this impedance can be efficiently implemented as an open-space impedance boundary condition (OSIBC) on the solution at Γ as if it is being solved on larger, or even infinite, domains.

Until about a decade ago, the use of impedance had been confined to solutions in the frequency domain and its description was principally a dependent variable of frequency $Z(\omega)$. The recent successes in the development of broadband impedance models [8–12] and their time-domain implementations as time-domain impedance boundary conditions for the solution of wave absorption/reflection problems inspired the extension of this concept to the treatment of all boundaries, physical or artificial. We will present various analytical open-space impedance (OSI) models and demonstrate their efficient implementation for accurate time-domain computation of waves in radiative and convective open spaces. We will then propose a general methodology for numerically defining the OSI of any finite domain intended for solutions of problems on open spaces and show how this methodology can be applied to existing schemes for solutions on truncated domains.

II. Wave and Impedance

Let $\phi_\infty(\vec{x}, t)$ be the target solution defined on an open infinite space, and let its initial value $\phi(\vec{x}, 0)$ be compactly supported; that is, $\phi(\vec{x}, 0)$ vanishes for $|\vec{x}| > R_0$ after some distance R_0 from the origin. For $0 < t < t_{\tilde{D}}$, the solution $\phi_\infty(\vec{x}, t)$, if achieved, should be exactly the same as that of $\tilde{\phi}(\vec{x}, t)$, solved on a truncated domain $\tilde{D}$ of boundary $\Gamma_{\tilde{D}}$ with the same initial value but with the boundary condition

$$\phi(\vec{x}, t)|_{\vec{x}\ \text{at}\ \Gamma_{\tilde{D}}} = 0$$

where $t_{\tilde{D}}$ is the minimum time that takes the initial value $\phi(\vec{x}, 0)$ to propagate from R_0 to $\Gamma_{\tilde{D}}$. If our interest, in practice, is approximations of $\phi_\infty(\vec{x}, t)$ for $t < t_{\tilde{D}}$ and over a domain D within $\tilde{D}$, the boundary condition

$$B\phi(\vec{x}, t)|_{\vec{x}\ \text{at}\ \Gamma} = 0$$

for solving $\phi(\vec{x}, t)$ on D should be derivable from $\tilde{\phi}(\vec{x}, t)$ and not necessarily related asymptotically to

$$\phi_\infty(\vec{x}, t)|_{\vec{x}\to\infty}$$

We will propose a way to construct the boundary operator B from the readily achievable reference solution $\tilde{\phi}(\vec{x}, t)$. Conversely, because all computations are finite in t, an appropriate $\tilde{D}$ can always be chosen for $\tilde{\phi}(\vec{x}, t)$ to define B for routine solutions of $\phi(\vec{x}, t)$ on any truncated D within $\tilde{D}$.

The classical approach to the solution $\phi(\vec{x}, t)$ of a space–time-varying problem $L\phi = 0$ on a domain D is through the Fourier/Laplace transform or the assumption of time-harmonic behavior, $\hat{\phi}(\vec{x}, \omega)e^{j\omega t}$. The determination of $\hat{\phi}(\vec{x}, \omega)$ then depends on the initial value $\phi(\vec{x}, 0)$ and the boundary condition as required by the spatial derivatives in the governing equation. If the governing equation of ϕ involves up to second spatial derivatives (in particular, ∇^2), the closure of the spatially elliptic problem requires constraints of the general form $a\hat{\phi} + b\hat{\phi}_n = 0$ at the contour Γ bounding the domain D. Here, the subscript n denotes a derivative or component normal to Γ and the coefficients a and b may assume all complex values, whereas they vary with ω. The solution of this boundary-value problem clearly depends on the ratio of b/a, which can be considered as a generalized form of impedance $Z(\omega, \Gamma)$, traditionally defined as the ratio between harmonic components of pressure p and velocity u_n normal to Γ.

To have a better appreciation of impedance and its relation to the reflectivity of a surface, consider the impingement of the advancing plane wave $\phi(x - t)$ [which satisfies the normalized two-dimensional wave equation $(\partial^2/\partial t^2 - \nabla^2)\phi = 0$] on an imagined inclined plane of angle θ. The corresponding pressure, x velocity, and y velocity, respectively, are $p \equiv -\phi_t$, $u \equiv \phi_x$, and $v \equiv \phi_y = 0$. This plane wave $\phi(x - t)$, however, is incomplete as a solution of the second-order wave equation, because the assumption of no receding wave, $\psi(x + t)$ or $u - p = 0$, is implicit. The velocity into the inclined plane of outward unit normal $\boldsymbol{n}$ is

$$\vec{u}_n = \vec{u} \cdot \boldsymbol{n} = u \sin\theta$$

which corresponds to the impedance of

$$Z = \frac{\hat{p}}{\hat{u}_n} = \frac{1}{\sin\theta}$$

For this inclined plane as a surface, the ratio of the domain-entering component $u^- = u_n - p$ to the domain-exiting component $u^+ = u_n + p$ forms the reflection coefficient $\hat{W} = \hat{u}^-/\hat{u}^+$, which can be bilinearly related to its impedance Z as

$$\hat{W} = \frac{1-Z}{1+Z} = \frac{\sin\theta - 1}{\sin\theta + 1}$$

Strictly by this definition, a surface of general orientation is not nonreflective (i.e., no domain-entering wave component $u^- = 0$), except for the normal plane of $\theta = \pi/2$. Therefore, the notion of a nonreflecting boundary for an outgoing wave is inappropriate in reference to this definition of $\hat{W}$, but the imposition of the reflective boundary condition

$$\hat{W} = \frac{\sin\theta - 1}{\sin\theta + 1}$$

ensures, in this case, the plane wave's free exit; that is, $\psi(x+t) = 0$. The fallacy, perhaps, is to associate and extend the asymptotic Sommerfeld radiation condition of $\lim_{r\to\infty}\psi(r+t) = 0$ to a finite distance at which, in general, $\psi(r+t) \neq 0$ in reference to the waves of a point source at $r = 0$. The real difficulty thus far is to specify the nontrivial domain-entering waves [e.g., $\psi(r+t)$] at an arbitrary bounding surface Γ, for which the domain of dependence is, unfortunately, exterior to Γ of D. We will show how to specific the OSI ($\hat{W}$ or Z) of a bounding surface Γ in an open space to ensure that the exiting waves are compatible with the nontrivial domain-entering waves.

We can now construct the reference solution $\tilde{\phi}(\vec{x}, t)$ that satisfies $L\tilde{\phi} = 0$,

$$\tilde{\phi}(\vec{x}, t)|_{\vec{x}\text{ at }\Gamma_{\tilde{D}}} = 0$$

or any homogeneous boundary condition, and

$$\tilde{\phi}(\vec{x}, 0) = \phi(\vec{x}, 0)$$

on a large, conveniently shaped, domain $\tilde{D}$ bounded by $\Gamma_{\tilde{D}}$ for which a set of orthonormal eigenvectors $e_k(\vec{x}, \omega_k)$ satisfying $\hat{L}e_k = 0$ and $e_k(\Gamma_{\tilde{D}}, \omega_k) = 0$ can be constructed to yield

$$\tilde{\phi}(\vec{x}, t) = \begin{cases} \sum_k A_k e^{j\omega_k t} e_k & 0 < t < t_{\tilde{D}} \\ 0 & 0 \geq t \text{ or } t \geq t_{\tilde{D}} \end{cases} \tag{1}$$

where $A_k = \langle \phi(\vec{x}, 0), e_k \rangle$, $\langle\ ,\ \rangle$ denotes some inner product, and $Le^{j\omega t} = e^{j\omega t}\hat{L}$. This reference solution is only conceptually needed to show the existence of $\tilde{\phi}(\vec{x}, t)$ for $\boldsymbol{x} \in D$ and $0 < t < \infty$. Thus, for an arbitrary (but small enough) contour Γ within $\Gamma_{\tilde{D}}$, the local normal-to-Γ incident $\hat{\tilde{\phi}}^+$ to reflected wave $\hat{\tilde{\phi}}^-$ of $\tilde{\phi}(\vec{x}, t)$ can then be constructed to define the open-space impedance $Z(\omega, \Gamma)$ or, equivalently, the open-space reflection coefficient

$$\hat{W} = \frac{\hat{\tilde{\phi}}^-}{\hat{\tilde{\phi}}^+} \tag{2}$$

In the following sections, we will show ways to define, approximate, construct, and implement various types of OSIBCs for numerical solutions on truncated domains.

III. Open-Space Impedances of Radiative and Convective Fields

A. Monopole OSI

The radiation of a monopole (Fig. 1) in two dimensions is described in the frequency domain $\omega(=kc)$ by the Hankel function $\hat{\phi} = H_0^{(2)}(kr)$, which corresponds to the radial impedance

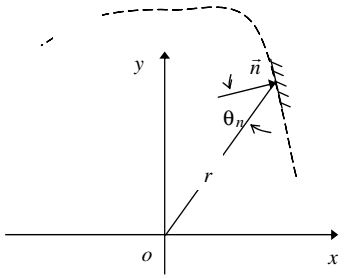

Fig. 1 Monopole at origin *O* radiating toward an arbitrary surface Γ of normal $\vec{n}$ at the distance *r* in an open space.

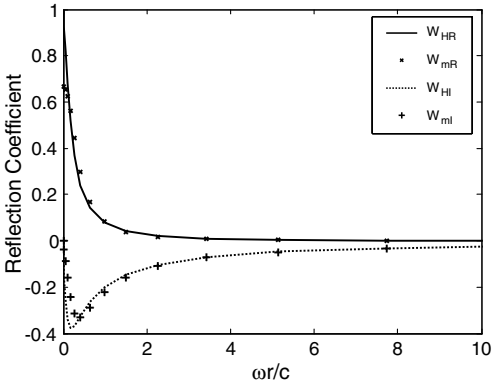

Fig. 2 Exact and modeled open-space reflection coefficients.

$$Z_m = \frac{p}{\rho_0 c u_r} = \frac{jH_0^{(2)}(kr)}{H_1^{(2)}(kr)} \tag{3}$$

and the reflection coefficient $\hat{W}_H$ shown in Fig. 2, in which its real part W_{HR} and imaginary part W_{HI}, $\mathrm{Im}(\hat{W}_H)$, are plotted against the dimensionless wave parameter kr or $\omega r/c$. The reflective behaviors of different harmonic components of the monopole are clearly frequency- and distance-dependent. Although both real and imaginary parts approach zero (nonreflective) asymptotically as $(kr)^{-1}$, albeit frequency-nonuniformly, the reflections (magnitude and phase) of waves of higher frequencies are smaller than those of lower frequencies at the same distance r from the origin of the monopole. At any fixed distance r, waves of the lowest frequencies ($kr < 1$) are highly reflective and phase-lagging. This reflection coefficient $\hat{W}_H$ is for the circular surface at a distance r from the monopole origin. For a general surface Γ for which the normal forms the incident angle θ_n with respect to the source (Fig. 1), the corresponding reflection coefficient $\hat{W}_\theta$ can be geometrically related to $\hat{W}_H$ by

$$\hat{W}_\theta = \frac{(\cos\theta_n - 1) + (\cos\theta_n + 1)\hat{W}_H}{(\cos\theta_n + 1) + (\cos\theta_n - 1)\hat{W}_H} \tag{4}$$

B. Implementation of OSIBCs

The key to the implementation of a time-domain impedance boundary condition is finding the poles of $\hat{W}_H$, which decay to zero at infinity and can be approximated as a sum of few (damped-harmonic-oscillator) DHO conjugate pairs [11,12] for a wide class of reflection coefficients; that is

$$\hat{W}_H \approx \hat{W}_m = \sum_k \hat{W}_k = \sum_k \frac{\mu_k}{s + \lambda_k} \tag{5}$$

where $s = j\omega$ is the Laplace variable. Each causal pole $\mathrm{Re}(\lambda_k) > 0$ of $\hat{W}_k$ corresponds to the time-domain reflection impulse

$$W_k(t) = \mu_k e^{-\lambda_k t} H(t)$$

with which the reflected wave $\phi^-(t)$ is related to the incident $\phi^+(t)$ at Γ by

$$\phi^-(t) = \sum_k \phi_k^-(t) \tag{6}$$

where

$$\phi_k^-(t) = \mu_k \int_0^\infty e^{-\lambda_k \tau} \phi^+(t-\tau)\, \mathrm{d}\tau$$

Equation (6) can be implemented in the time domain as the two-level unconditionally stable recursive scheme with $z_k = e^{-\lambda_k \Delta t}$:

$$\phi_k^-(t) = \mu_k[\phi^+(t) + z_k \phi^+(t-\Delta t)]\frac{\Delta t}{2} + z_k \phi_k^-(t-\Delta t) \tag{7}$$

Equation (7) is crucial in that it recursively imposes on $\phi(t)$ and pointwisely imposes on Γ conditions that are traceable or derivable from the solution interior to Γ and before t, without reference to any exterior condition. This implementation genuinely reflects the mathematical nature of the initial-valued hyperbolic radiation problem. It is important to note that Eq. (4) is in the form of

$$\hat{W}_\theta = \frac{A + B\hat{W}_H}{C + D\hat{W}_H} \tag{8}$$

The corresponding reflection impulse $W_\theta(t)$ of Eq. (8) with $\hat{W}_m$ assumed and its distinct poles known [Eq. (5)] may be approximated by

$$\hat{W}_\theta \approx \frac{A}{C} + \sum_k \lim_{a_k s \to -b_k} \frac{B - AD/C}{(a_k s + b_k)C + D} \tag{9}$$

Thus, $W_\theta(t)$ may assume the form

$$\begin{aligned} W_\theta &= \frac{A\delta(t)}{C} + \sum_k \left(\frac{(B - AD/C)e^{-(b_k + \frac{D}{C})\frac{t}{a_k}}}{a_k C} \right) \\ &= \frac{A\delta(t)}{C} + \sum_k \mu_k e^{-\lambda_k t} \end{aligned} \tag{10}$$

and can be implemented by Eqs. (6) and (7) as OSIBCs. It is interesting to note that the first term A/C on the right-hand side of Eq. (9) corresponds to the reflection coefficient of a plane wave:

$$\hat{W}_{\tilde{\theta}} = \frac{\cos\theta_n - 1}{1 + \cos\theta_n}$$

which is the high-frequency limit of $\hat{W}_\theta$ in Eq. (8). And it is rather surprising to find that the simple model

$$\hat{W}_m = \frac{1}{4s + 1.5} \tag{11}$$

for which the real and imaginary parts W_{mR} and W_{mI} are plotted with their analytic values in Fig. 2, well represents $\hat{W}_H$ for $kr > 0.5$. This model greatly facilitates the implementation of OSIBCs for radiative fields.

Figure 3 compares the pressure contours, set with a range of 11 levels in increments of 0.015 from -0.097, of the radiation of an initially Gaussian pressure pulse $p(x, y, 0) = e^{-\ell_n 2(r/5)^2}$ on a $[-50, 50] \times [-50, 50]$ rectangular grid $\Delta x = \Delta y = 8\Delta t = 1$ at $t = 70$ (grid points traveled). The pressure contours are computed in Fig. 3a with the no-reflection condition $\hat{W} = 0$, in Fig. 3b with the plane-wave reflection coefficient $\hat{W}_{\tilde{\theta}}$, and in Fig. 3c with the broadband one-pole model $\hat{W}_m$ of Eq. (11). This and the subsequent demonstrations were obtained by a straightforward specification of the domain-entering waves on the C3N wave solvers of Fung [13] for the dimensionally split multidimensional linearized Euler equations. Although the improvement due to the plane-wave effect is clearly shown in Fig. 3b, the importance of preserving low-frequency, phase-lagging, domain-exiting reflections is evident in Fig. 3c. Figure 4 compares the same contours as in Fig. 3c, but computed on an off-center grid $[-55, 45] \times [-45, 53]$, showing the effectiveness of OSIBCs and showing excellent agreement with contours computed on the larger $[-70, 70] \times [-70, 70]$ grid.

C. Dipole OSI

Although pulsating sources or compactly initialized solutions can be modeled as monopoles, dipoles (as various combinations of monopoles) are often used to model the effect of closed bodies. The monopole is purely radial (i.e., $u_\theta = 0$). Dipoles are directional, with an angular variation of $u_\theta(r, \theta, t)$ with respect to the dipole axis. It is important to learn how such OSI can be constructed. Figure 5 shows the placement of two monopoles on the x axis separated at a distance of $2a$. If other orientations are used, the measurement of θ could be appropriately defined, rather than using its assumed reference with the x axis. The combined impedance has the form

$$Z_d = \frac{p_1 + p_2}{u_1 \cos\theta_1 + u_2 \cos\theta_2} = \frac{Z_m(kr_1)u_1 + Z_m(kr_2)u_2}{u_1 \cos\theta_1 + u_2 \cos\theta_2} \tag{12}$$

In the limit of $a \to 0$ and $u_1 = -u_2$,

$$Z_{d\theta} = \frac{s}{(sZ_m + 1 - \tan^2\theta)\cos\theta} \tag{13}$$

Because the poles of $\hat{W}_{d\theta}$ are the zeros of $1 + Z_{d\theta}$, $\hat{W}_{d\theta}$ has an additional pole compared with $\hat{W}_m$, due to the term sZ_m in the denominator of Eq. (13).

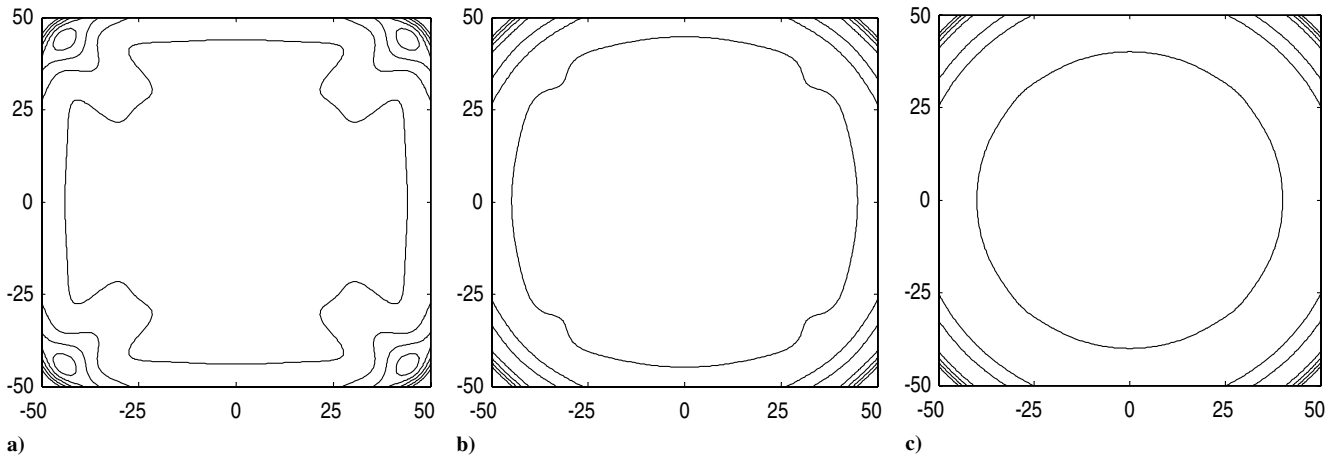

Fig. 3 Pressure contours of computed pulses with a) $\hat{W} = 0$, b) plane wave $\hat{W}_{\tilde{\theta}}$, and c) OSIBC of Eq. (11).

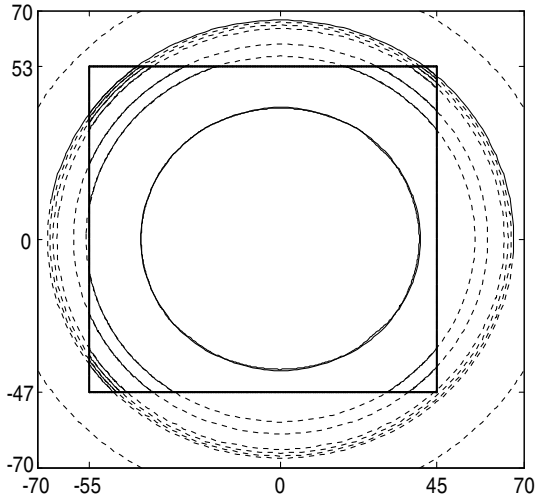

Fig. 4 Demonstration of OSIBC effectiveness computed on a large grid (dotted) and on the inset smaller grid (solid).

D. Convective OSI

An important application of OSIBCs is the convective flow. Through the Prandt–Glauert transformation, the linearized Euler equation can be mapped to the Helmholtz equation and the response can be mapped to an impulse $L\phi(r,0)=\delta(r)$ to the Hankel function, to yield the convective acoustic potential

$$\phi=\left(\frac{j}{4\beta}\right)e^{-j\beta^{-2}Mkr\cos\theta}H_0^{(2)}(\alpha\beta^{-2}kr) \tag{14}$$

the convective impedance

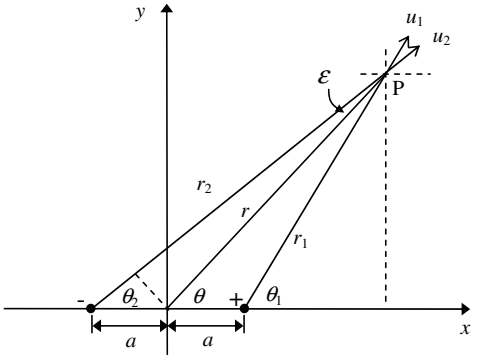

Fig. 5 Dipole and orientations.

$$Z_M=\frac{\alpha M\cos\theta-Z_m}{Z_m M\cos\xi-\alpha\vartheta} \tag{15}$$

and the corresponding convective reflection coefficient

$$\hat{W}_M=\frac{\vartheta-\alpha-(\alpha\cos\xi-\cos\theta)M+[\vartheta+\alpha+(\alpha\cos\xi+\cos\theta)M]\hat{W}_m}{\vartheta+\alpha-(\alpha\cos\xi+\cos\theta)M+[\vartheta-\alpha+(\alpha\cos\xi-\cos\theta)M]\hat{W}_m} \tag{16}$$

of the convecting impulse radiating in an open space, where

$$\vartheta=\cos\theta\cos\xi+\beta^2\sin\theta\cos\zeta$$

$\cos\xi=\vec{n}\cdot\boldsymbol{i}$, and $\cos\varsigma=\vec{n}\cdot\boldsymbol{j}$; the latter two are the direction cosines of a boundary surface at a distance r and angle θ from the origin. Equation (16) is in the same form as Eq. (8) and can be similarly implemented as OSIBCs, per Eq. (10).

Figure 6 compares the pressure contours, again in increments of 0.015, of the radiation of the initially Gaussian pulse

$$p(r,0)=e^{-r^2\ln 2/6}$$

on a $[-30,30]\times[-30,30]$ rectangular grid at $t=40$ (grid points traveled). The pressure contours are computed in Fig. 6a with the no-reflection condition $\hat{W}=0$, in Fig. 6b with plane wave $\hat{W}_{\tilde{\theta}}$, and in Fig. 6c with Eq. (16) and the broadband one-pole model $\hat{W}_m$ of Eq. (11). The results confirm, as before, the importance of the preservation of low-frequency reflection. Here, a narrower, marginally resolved, Gaussian pulse $e^{-r^2\ln 2/6}$ (for which the half-width radius spans $\sqrt{6}\approx 2.45$ grid points) was used instead of the half-width radius 5 in Fig. 3. The use of a shorter pulse affects the smoothness of the circular contours in Fig. 6c. If a wider and smoother pulse is used, local spurious reflections can easily be detected from the deviated circular contours of the radiating pulse.

This deviation problem can be grasped by noting the following:

1) The initially Gaussian pressure pulse $p(r,0)=e^{-r^2\ln 2/6}$ is not concentrated, as assumed for Eq. (14), but is composed of distributed sources of magnitude $e^{-r^2\ln 2/b^2}$ over the half-width radius b of the initially Gaussian distribution.

2) Equation (16), the OSI for boundary points at various distances from the sources, is a highly complex and sensitive function of θ, which measures the angles of a boundary point with respect to the various origins of the distributed sources as they convect.

The pressure field $p(r_A,t,b,M)$ of a distributed source initially centered at the coordinate origin O (Fig. 7) radiates, convects, and reaches the fixed point $A(x_A,y_A)$ in the Eulerian reference as the source center convects from O at $x=0$ to O_1 at $x=Mct$. This pressure is exactly the same as $p(r_B,t,b,0)$ for a stationary source of $M=0$ radiating from O_1, where

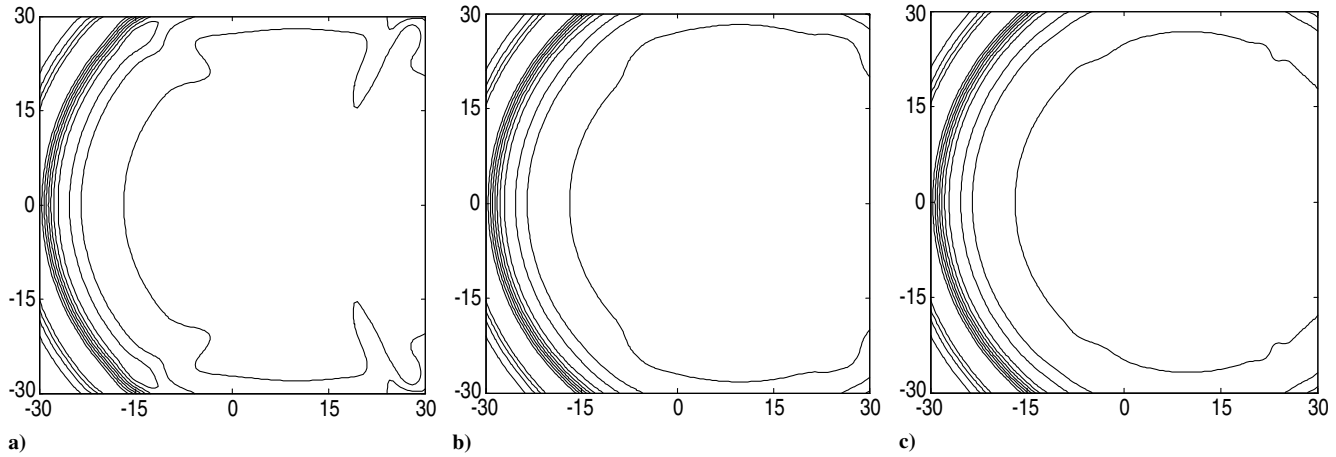

Fig. 6 Pressure contours of computed pulses of $M=0.25$ with a) $\hat{W}=0$, b) plane wave $\hat{W}_{\tilde{\theta}}$, and c) OSIBC of Eq. (16).

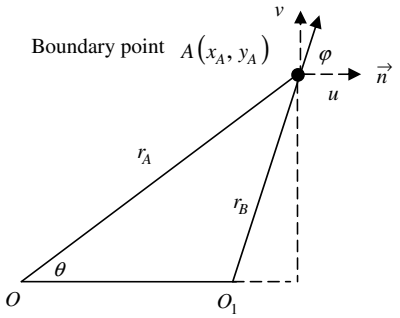

Fig. 7 The pressure front A reaches distance r_A as the center of a distributed source reaches O_1.

$$\vec{r}_A = Mct\vec{i} + \vec{r}_B(t)$$

which, in two dimensions, is

$$p(r_B, t, b, 0) = \left(\frac{r_A}{r_B}\right)^{\frac{1}{2}} p\left(r_A, t + \frac{r_A - r_B}{c}, b, 0\right)$$

asymptotically for large r; hence,

$$p(r_A, t, b, M) = \left(\frac{r_A}{r_B}\right)^{\frac{1}{2}} p\left(r_A, t + \frac{r_A - r_B}{c}, b, 0\right) \tag{17}$$

Similarly, the corresponding perturbed flow speed $q(r_A, t, b, M)$ of the convecting source can be related to that of the stationary source as

$$q(r_A, t, b, M) = \left(\frac{r_A}{r_B}\right)^{\frac{1}{2}} q\left(r_A, t + \frac{r_A - r_B}{c}, b, 0\right) \tag{18}$$

and its flow angle measured radially from O_I increases from θ to φ as

$$\cos\varphi = \frac{r_A \cos\theta - Mct}{r_B}$$

or

$$\sin\varphi = \frac{r_A \sin\theta}{r_B}$$

To a surface of $\vec{n} = \cos\xi\vec{i} + \cos\varsigma\vec{j}$ (Fig. 1), its impedance has the form

$$Z_{M,b} = \frac{\hat{p}(r_A, \omega, b, M)}{\overbrace{q(r_A, \omega, b, M)\cos\bar{\varphi}}^{\wedge}} \tag{19}$$

where

$$\cos\bar{\varphi} = \cos\varphi|\cos\zeta| + \sin\varphi|\cos\xi|$$

and can be approximated as

$$\frac{\overbrace{(\sigma_0 + \sigma_1 t + \cdots)p(r_A, \gamma t - t_{ox}, b, 0)}^{\wedge}}{\overbrace{(\vartheta_0 + \vartheta_1 t + \cdots)q(r_A, \gamma t - t_{ox}, b, 0)}^{\wedge}}$$

or operationally expressed as

$$Z_{M,b} = \left(\sigma_0 + j\sigma_1\frac{\partial}{\partial\omega} - \sigma_2\frac{\partial^2}{\partial\omega^2}\cdots\right)\frac{e^{-j\omega t_{ox}/\gamma}\hat{p}_0(\omega/\gamma)}{\gamma} \Bigg/ \left(\vartheta_0 + j\vartheta_1\frac{\partial}{\partial\omega} - \vartheta_2\frac{\partial^2}{\partial\omega^2}\cdots\right)\frac{e^{-j\omega t_{ox}/\gamma}\hat{q}_0(\omega/\gamma)}{\gamma} \tag{20}$$

and related to the monopole impedance of Eq. (3) by

$$Z_{M,b} = \frac{Z_m(\omega/\gamma)(\kappa_1 + j\kappa_2\omega)}{\kappa_3 + j\kappa_4\omega} \tag{21}$$

The expressions of ϑ_i, σ_i, and κ_i in terms of (r, θ, b, M) are derived in the Appendix. The form of Eq. (21) suggests that the corresponding reflection coefficients $\hat{W}_{M,b}$ can be related to $\hat{W}_m$ of Eq. (5) by a quotient of polynomials in ω that is one order higher than that in Eq. (8) or by the addition of one pole to Eq. (10); that is,

$$\hat{W}_{M,b} \approx \frac{(\kappa_3 + j\kappa_4\omega)(1 + \hat{W}_m) - (\kappa_1 + j\kappa_2\omega)(1 - \hat{W}_m)}{(\kappa_3 + j\kappa_4\omega)(1 + \hat{W}_m) + (\kappa_1 + j\kappa_2\omega)(1 + \hat{W}_m)} \tag{22}$$

The principal role of the additional pole is to account for the apparent wave-speed and directional changes of a domain-exiting wave as it leaves an artificially truncated boundary of an open space.

Figure 8a compares the computed pressure with the same initial pulse of half-width radius 5 as in Fig. 3, but for $M = 0.5$ at $t = 40$ on a sufficiently large grid (dashed contours) and on a small grid (solid contours) of $[-30, 30] \times [-30, 30]$. Figure 8a shows the effectiveness of Eq. (22), and Fig. 8b shows the inadequacy of Eq. (16) in accounting for the wave-speed and directional changes of the domain-exiting waves.

IV. Applicability of and General Procedures for OSIBCs

As the complexity of a numerical solution increases, the analytic structure of OSI may not be readily available or easily discerned. We propose a general methodology specifically for the reduction of the size of a grid on any existing algorithm. The procedures are as follows:

1) Pick any existing numerical scheme for a particular problem.

2) Initialize some suitable, convenient, compactly supported distribution of solution nonuniformities (e.g., space–time Gaussian pulses) in space–time in the inner region of an existing grid.

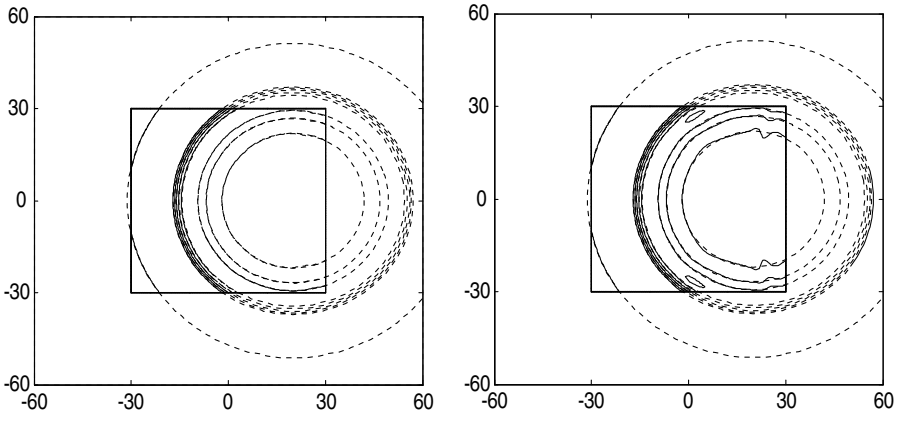

Fig. 8 Pressure contours of $M = 0.5$ computed on the inset small grid (solid) and on a large grid (dashed) with the a) OSIBC of Eq. (22) and b) OSIBC of Eq. (16) .

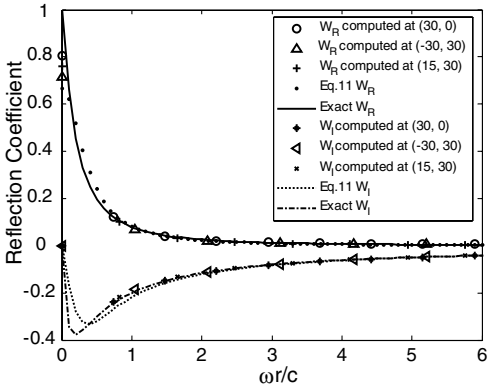

Fig. 9 Comparison of computed and fitted monopole OSI models $\mathbf{Re}(\hat{W}) = W_R$ and $\mathbf{Im}(\hat{W}) = W_I$.

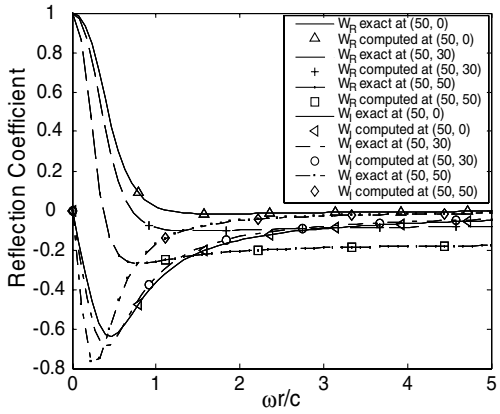

Fig. 10 Comparison of computed and fitted dipole OSI models $\mathbf{Re}(\hat{W}) = W_R$ and $\mathbf{Im}(\hat{W}) = W_I$.

3) Advance the scheme and allow the nonuniformities to propagate outwardly just before their fronts reach the outermost grid surface Γ_N or before their reflections reach the target boundary $\Gamma_n (n < N)$.

4) Store the time sequences of all incoming and outgoing characteristic variables (wave components, pressure wave, vorticity wave, etc.) on and normal to the interior grid plane Γ_n.

5) Eliminate the solution's dependence on the domain-entering wave components by forming appropriately defined OSI, Z or $\hat{W}_n$, from the stored sequences. This is always possible, because a complete finite-time solution to an equation model of the hyperbolic type (having a finite domain of spatial dependence such as a time-marching scheme for the Navier–Stokes equations) has already been obtained.

6) Numerically fit and convert $\hat{W}_n$ constraints relating the domain-entering to the domain-exiting wave components to a series of damped harmonic oscillators (DHO) or their time-domain impulses

$$\sum_k \mu_k e^{-\lambda_k t}$$

7) Set Γ_N to Γ_n with the corresponding OSIBC.

Figure 9 compares the reflection coefficients evaluated at the points (30,0), (15,30), and $(-30, 30)$ from the solution on the large $[-150, 150] \times [-150, 150]$ grid, showing excellent agreement with the analytical $\hat{W}_H$ of the infinite open space. Figure 10 compares, on the same large grid, the numerically computed reflection coefficients of a dipole (oriented at 25 deg) evaluated for points (50,0), (50,30), and (50,50), showing not only the excellent agreement with Eq. (13), but also the sensitive angular dependence of $\mathrm{Im}(\hat{W}_{d\theta})$.

Because the dipole decays faster than the monopole, the implementation of the dipole OSIBC for the computed contours of Fig. 11c on the $[-10, 10] \times [-10, 10]$ inset grid shows a slight improvement over those of Fig. 11b computed for the dipole source but with the monopole OSIBC of Eq. (11) and, clearly, the inadequacy of the plane wave $\hat{W}_{\bar{\theta}}$ in Fig. 11a. These results suggest that an appropriate choice of OSIBC is rather flexible, depending on the solution objective. The monopole OSIBC is not a poor approximation for the dipole and therefore all higher-order poles. Although the plane wave $\hat{W}_{\bar{\theta}}$, the first term on the right-hand side of Eq. (9), may be appropriate for most high-frequency components (e.g., Fig. 6b), the subsequent DHO poles are important for the space–time accuracy of the lower-frequency components.

The fact that these results scale with $\omega r/c$ suggests that an OSI obtained by the Fourier transform of a time sequence of the solution on a finite domain can be extended to solutions on larger or even infinite domains. The OSI correctly casts the domain-entering waves (for which the domain of dependence is exterior to the truncated domain of interest) in terms of the domain-exiting waves as an initial-value problem, per Eq. (7), rather than subjecting the domain-entering waves to an asymptotic Sommerfeld-like constraint as a boundary-value problem. This approach preserves the initial-value nature of the radiation (hyperbolic) problem by a simple extension of the finite-time-period solution characteristics and their Fourier transforms [Eqs. (1) and (2)] to respective infinite-time-period solution characteristics, rather than solving it as a formidable boundary-value-problem of infinite spatial extent. In principle, a strategy could be devised to employ the OSI obtained for an interior boundary Γ_n to the outmost boundary Γ_N before the front reaches it. The form of $\hat{W}_n$ as a series of DHOs also suggests the advantageous selection and addition of terms as dampers or filters to bands of waves (physical or spurious) by design, which is beyond the scope of our work here.

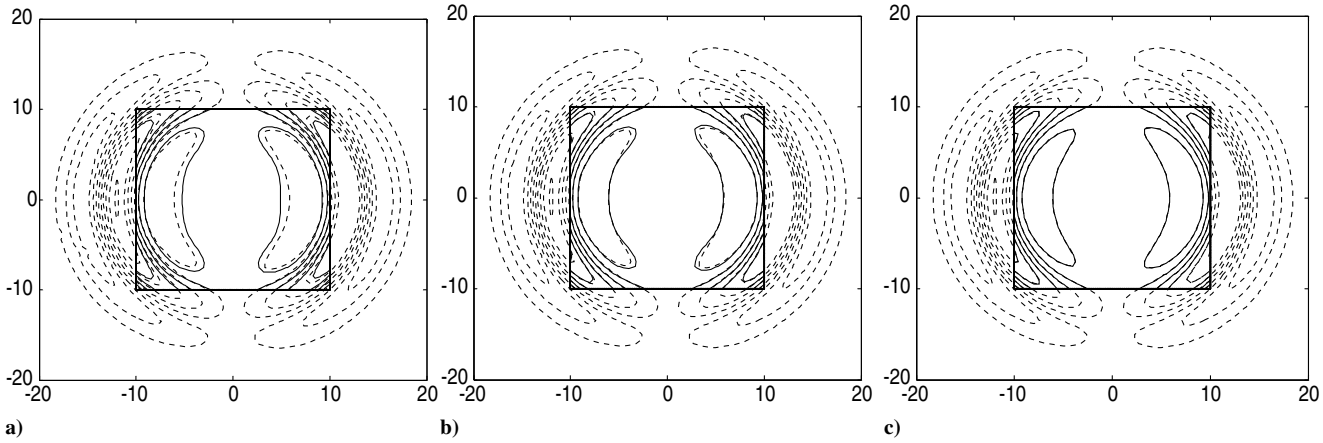

Fig. 11 Pressure contours of dipole pulses computed on the inset small grid (solid) and on a large grid (dashed) with the a) plane wave $\hat{W}_{\bar{\theta}}$, b) monopole OSIBC and c) dipole OSIBC.

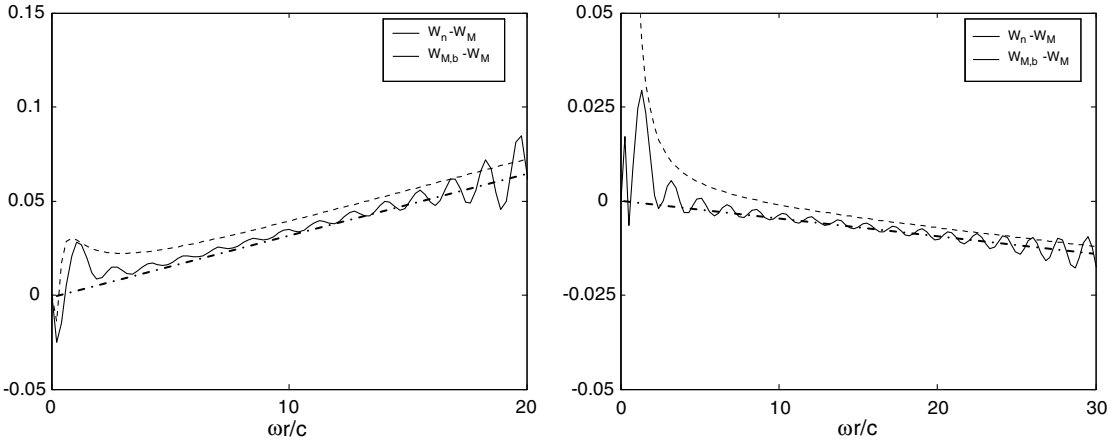

Fig. 12 Comparison of $\mathrm{Im}(\hat{W}_{M,b} - \hat{W}_M)$ and $\mathrm{Im}(\hat{W}_n - \hat{W}_M)$ at boundary points a) (0, 30) and b) (20,30).

Figures 12a and 12b show how, in practice, the effects due to pulse width b and convection M on $\hat{W}_{M,b}$ can be numerically studied by computing $\hat{W}_n$ (solid lines in Fig. 12) for various M and b on a large enough grid (here, $[-120, 120] \times [-120, 120]$) fitted as an approximation to $\hat{W}_{M,b}$ (dashed lines in Fig. 12) and implemented for OSIBC applications, as already illustrated in Fig. 8a. A comparison of $\hat{W}_M$ of Eq. (16) with the numerically computed $\hat{W}_n$ and with $\hat{W}_{M,b}$ of Eq. (22) for the boundary point (0, 30) (Fig. 12a) and for (20, 30) (Fig. 12b) on Γ_n of the reduced computational domain $[-30, 30] \times [-30, 30]$ reveals that the principal difference is the addition of a term of the form $j\omega g(M, b, \Gamma_n)$ (dotted-dashed lines in Fig. 12), which was numerically fitted and applied for the result in Fig. 8a. The ω dependence of this purely imaginary term (Fig. 12) shows a way to account for phase-sensitive differences in an OSIBC that are due to locally varying wave speed and angle as waves exit Γ_n.

It should be noted here that caution be taken in the choice of possibly noncausal approximations to $\hat{W}_{M,b}$. Although, in theory, OSI models such as Eq. (19) derived from causal processes are often causal, their approximations [e.g., Eq. (21)] for implementation may be noncausal and only conditionally stable [10,11]. So far, all the OSI expressions, except Eq. (21), are causal and implemented as [Eq. (7)] unconditionally stable for indefinite calculations. Because the additional term in Eq. (21) at the low-frequency end behaves as $j\omega$ (dotted-dashed line in Fig. 12), which is noncausal for the corresponding pole at $\omega \to \infty$ and can be implemented as a time derivative requiring finite, but not arbitrarily small, time steps to avoid amplification of high-frequency spurious waves in the solution algorithm [10,11]. Better approximations may be possible, but at the expense of algorithmic and analytic simplicity. Figure 13 shows a subsequent frame of pressure contours that is similar to that in Fig. 8, but computed to $t = 200$. The pressure contours are computed in Fig. 13a with the no-reflection condition, in Fig. 13b with the plane-wave high-frequency limit of Eq. (16), and in Fig. 13c with the OSIBC of Eq. (21). Only the almost-straight, barely visible (shown by a factor of 10^{-2} lower than the contour levels in previous figures) residue-level (10^{-4}) contours in Fig. 13c resemble the remnants of an expanded convected pulse, whereas spurious reflections resulted from the incompatible boundary conditions are evident in both Figs. 13a and 13b. Because the C3N algorithm used is numerically nondissipative [13], longer-time or indefinite continuations of all the preceding cases (regardless of the OSIBC) have resulted in decreasing spurious residue remnants.

It may also be of interest to note that the broadband OSI models presented here are applicable not only for transient or finite-time-period computations but also for time-indefinite computations. The broadband initial pressure pulses were replaced by harmonic sources for indefinite computations on truncated domains and can simply be replaced by periodic or general time-varying sources with the same broadband OSIBC derived from an initial pressure distribution as the source. An OSI model so derived contains the basic phase-space characteristics of a type of source emanating into an open space. Its frequency $\omega r/c$ range of applicability varies from the lowest $2\pi/T$ to the Nyquist cutoff $\pi/\Delta t$ for a set of $T/\Delta t$ FFT data sample. The development of OSI models for problems with local complexities would, however, depend on whether a Green's function can be meaningfully formulated and practically constructed either analytically or numerically, which is beyond our scope here.

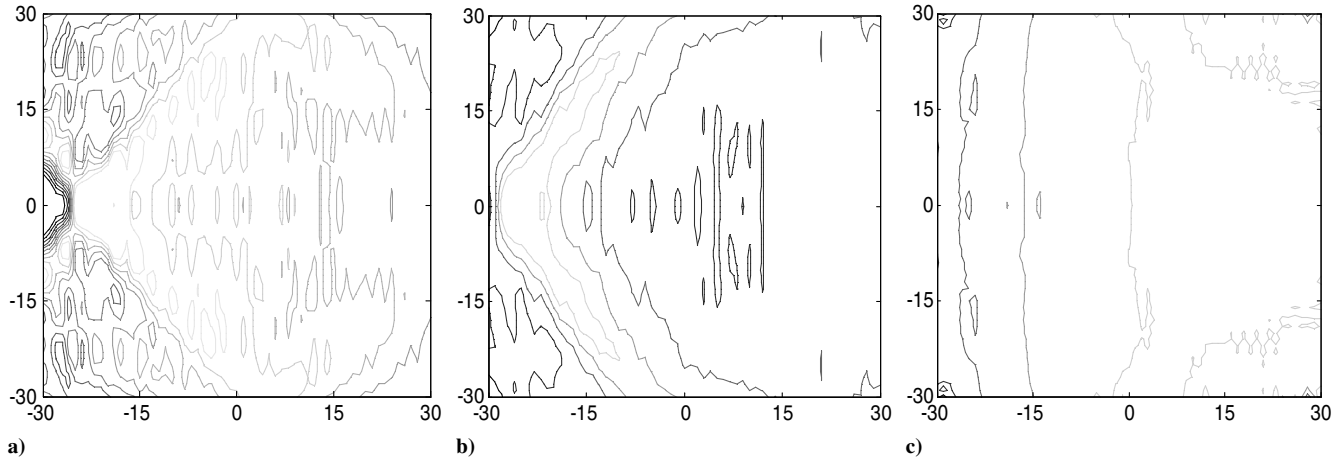

Fig. 13 Scaled up (by 10^{-2}) remnant pressure contours of the computed pulses of $M = 0.5$ at $t = 200$ with a) $\hat{W} = 0$, b) plane wave $\hat{W}_{\bar{\theta}}$, and c) OSIBC of Eq. (22).

V. Conclusions

We outlined a new and general approach for the definition of OSI for numerical solution of problems originally formulated on an infinite open space but computed over finite-time periods and on truncated domains. We have shown the analytic structures and dependence of OSI on distance, frequency, surface orientation, type of sources, convection, and variations of wave speed and angle. We have outlined ways to analyze, study, and implement OSIBCs for various types of sources and demonstrated the effectiveness of OSIBCs for stationary and convecting monopoles. We also proposed a general methodology for the definition of OSI on existing algorithms, discussed its extendability and validity, and provided practical examples of OSIBCs for computations on reduced domains.

Appendix: OSI of Convecting Monopoles

After coordinate transformation to the moving center

$$Mcti = \vec{r}_A - \vec{r}_B(t)$$

the pressure

$$p_M \equiv p(\vec{r}_A, t, b, M)$$

and total velocity

$$q_M \equiv q(\vec{r}_A, t, b, M)$$

at a fixed point A due to a convecting monopole of Mach number M, Gaussian half-width b initially centered about the reference-frame origin O at $r = 0$ resumes the form $p(\vec{r}_B, t, b, 0)$ and $q(\vec{r}_B, t, b, 0)$ of a respective stationary monopole, which radiates symmetrically along characteristics $\vec{r}_B - ct$ about the moving origin O_1 (Fig. 7) and decays asymptotically as $r^{-\frac{1}{2}}$; that is,

$$f(\vec{r}, t, b, 0) \sim r^{-\frac{1}{2}} f_0(\vec{r} - ct)$$

At far distances from the origin, $p(\vec{r}_B, t, b, 0)$ can be related to

$$\left(\frac{r_A}{r_B}\right)^{\frac{1}{2}} p\left(r_A, t + \frac{r_A - r_B}{c}, b, 0\right)$$

and approximated as

$$p_M(t) \approx (\sigma_0 + \sigma_1 t) p_0(\gamma t - t_{ox})$$

where

$$t + \frac{r_A - r_B}{c} \approx \gamma t - t_{ox}$$

$$t_{ox} = \frac{r_A \alpha(\alpha - M\cos\theta - \beta^2) - r_A(M^2\alpha - M\cos\theta)}{\alpha\beta^2 c}$$

$$\gamma = 1 - \frac{(M^2\alpha - M\cos\theta)(1 + M\cos\bar{\varphi})}{\alpha\beta^2}$$

$$\cos\bar{\varphi} = \frac{\cos\theta - Mc}{\sqrt{1 + M^2c^2 - 2Mc\cos\theta}}$$

$$\sigma_0 = \sqrt{\frac{r_A}{T_c c}}\,\frac{1 + (1-\gamma)T}{2T_c}$$

$$\sigma_1 = \frac{-(1-\gamma)\sqrt{r_A/T_c c}}{2T_c}$$

$$\sigma_2 = \frac{r_A[T_a + 2(1-\gamma)T]}{T_c^2 c}$$

$$\sigma_3 = \frac{(\gamma - 1)r_A}{T_c^2 c}$$

$$T = \frac{\sqrt{r_A^2 M^2\cos^2\theta + \beta^2 r_A^2} - r_A M\cos\theta}{\beta^2 c}$$

$$T_a = t_{ox} - (r_A/c)$$

$$T_c = T_a + (1-\gamma)T$$

Similarly,

$$q_M(t)\cos(\varphi - \theta) \approx (\vartheta_0 + \vartheta_1 t + \vartheta_2 t^2 + \vartheta_3 t^3) q_0(\gamma t - t_{ox})$$

where

$$\vartheta_0 = \sigma_0\sigma_2(\cos\theta|\cos\zeta| + \sin\theta|\cos\xi|)$$

$$\vartheta_1 = \sigma_0\sigma_3\cos\theta|\cos\zeta| - \frac{\sigma_0\sigma_2 Mc|\cos\zeta|}{r_A} + \sigma_0\sigma_3\sin\theta|\cos\xi| + \sigma_1\sigma_2(\cos\theta|\cos\zeta| + \sin\theta|\cos\xi|)$$

$$\vartheta_2 = \sigma_1\sigma_3(\cos\theta|\cos\zeta| + \sin\theta|\cos\xi|) - \frac{Mc(\sigma_1\sigma_2|\cos\zeta| + \sigma_0\sigma_3|\cos\zeta|)}{r_A}$$

$$\vartheta_3 = \frac{-\sigma_1\sigma_3 Mc|\cos\zeta|}{r_A}$$

The transformed pressure of an initially Gaussian pulse has the form

$$p_0\left(\frac{\omega r}{c}\right) = \frac{\omega\pi H_0^{(2)}(wr/c)e^{-\frac{\omega^2}{4b}}}{4bc}$$

and the corresponding total velocity has the form

$$q_0\left(\frac{\omega r}{c}\right) = \frac{j\omega\pi H_1^{(2)}(\omega r/c)e^{-\frac{\omega^2}{4b}}}{4bc}$$

Regardless of the compact initial Gaussian distribution of half-width b, the open-space impedance $Z_{0,b} = p_0/q_0$ derived from the response to a finite-width initially Gaussian pulse is exactly the same as the Z_m of Eq. (3) derived from the response to the infinitely sharp delta function. Hence, the OSI of the convecting monopole $Z_{M,b} = \hat{p}_M/\hat{q}_M$ is of the form of Eq. (20), of which both numerator and denominator involve terms of

$$\frac{\partial e^{-j\omega t_{ox}} f(\omega)}{\partial\omega}$$

or

$$e^{-j\omega t_{ox}}\left(f\frac{\mathrm{d}\,\ell n\, f}{\mathrm{d}\omega} - jt_{ox}f\right)$$

Because

$$\frac{\mathrm{d}\,\ell n\, p_0(\omega)}{\mathrm{d}\omega} = \frac{1}{\omega} + \frac{rH_1^{(2)}}{H_0^{(2)}} - \frac{\omega}{2b}$$

approaching $(jr/c) - (\omega/2b)$ for $\omega > 0$ and $\hat{q}_0$ can be expressed as $\hat{p}_0/Z_m$, the rational expansion of Eq. (20) then leads to Eq. (21),

where

$$\kappa_1 = \frac{\sigma_0\gamma + \sigma_1[t_{ox} + (r/c)]}{\gamma^2}$$

$$\kappa_2 = \frac{-\sigma_1}{2br\gamma^2}$$

$$\kappa_3 = \frac{(\vartheta_0\gamma + \vartheta_1 t_{ox})\gamma^2 + \vartheta_2 t_{ox}^2\gamma + \vartheta_3 t_{ox}^3 + r\left(\vartheta_1\gamma^2 + 2t_{ox}\vartheta_2\gamma + 3\vartheta_3 t_{ox}^2\right) + r^2(\vartheta_2\gamma + 3\vartheta_3 t_{ox}) + r^3\vartheta_3}{\gamma^4}$$

$$\kappa_4 = -\frac{\vartheta_1\gamma^2 + 2t_{ox}\vartheta_2\gamma + 3\vartheta_3 t_{ox}^2}{2br\gamma^5} - \frac{2(\vartheta_2\gamma + 3\vartheta_3 t_{ox}) + 4r\vartheta_3}{2b\gamma^5}$$

Acknowledgment

Financial support of the Hong Kong Research Grants Council's Competitive Earmarked Research Grant PolyU 5296/03E is gratefully acknowledged. The authors are grateful to the reviewers' many helpful comments and suggestions.

References

[1] Givoli, D., "Non-Reflecting Boundary Conditions," *Journal of Computational Physics*, Vol. 94, May 1991, pp. 1–29. doi:10.1016/0021-9991(91)90135-8

[2] Tsynkov, S. V., "Numerical Solution of Problems on Unbounded Domains: A Review," *Applied Numerical Mathematics*, Vol. 27, Aug. 1998, pp. 465–532. doi:10.1016/S0168-9274(98)00025-7

[3] Hu, F. Q., "Absorbing Boundary Conditions," *International Journal of Computational Fluid Dynamics*, Vol. 18, No. 6, 2004, pp. 513–522. doi:10.1080/10618560410001673524

[4] Thompson, K. W., "Time-Dependent Boundary Conditions for Hyperbolic Systems, 2," *Journal of Computational Physics*, Vol. 89, Aug. 1990, pp. 439–461. doi:10.1016/0021-9991(90)90152-Q

[5] Engquist, B., and Majda, A., "Absorbing Boundary Conditions for the Numerical Simulation of Waves," *Mathematics of Computation*, Vol. 31, No. 139, 1977, pp. 629–651. doi:10.2307/2005997

[6] Bayliss, A., and Turkel, E., "Radiation Boundary Conditions for Wave-Like Equations," *Communications on Pure and Applied Mathematics*, Vol. 33, No. 6, 1980, pp. 707–725. doi:10.1002/cpa.3160330603

[7] Grote, M. J., and Keller, J. B., "Nonreflecting Boundary Conditions for Time-Dependent Scattering," *Journal of Computational Physics*, Vol. 127, Aug. 1996, pp. 52–65. doi:10.1006/jcph.1996.0157

[8] Tam, C. K. W., and Auriault, L., "Time-Domain Impedance Boundary Conditions for Computational Acoustics," *AIAA Journal*, Vol. 34, No. 5, 1996, pp. 917–923.

[9] Özyörük, Y., and Long, L. N., "A Time-Domain Implementation of Surface Acoustic Impedance Condition with and Without Flow," *Journal of Computational Acoustics*, Vol. 5, No. 3, 1997, pp. 277–296. doi:10.1142/S0218396X97000162

[10] Fung, K.-Y., Ju, H. B., and Tallapragada, B., "Impedance and Its Time-Domain Extensions," *AIAA Journal*, Vol. 38, No. 1, 2000, pp. 30–38.

[11] Fung, K.-Y., and Ju, H. B., "Time-Domain Impedance Boundary Conditions for Computational Acoustics and Aeroacoustics," *International Journal of Computational Fluid Dynamics*, Vol. 18, No. 6, 2004, pp. 503–511. doi:10.1080/10618560410001673515

[12] Fung, K.-Y., and Jing, X. D., "Characterization of Impedance Boundary as Damped Harmonic Oscillators Via Impulse Reflection," *Journal of the Acoustical Society of America*, Vol. 119, No. 6, 2006, pp. 3831–3838. doi:10.1121/1.2198185

[13] Fung, K.-Y., "Time-Domain Computation of Acoustics with Realistic Geometry and Impedance Boundary Condition," *Advances in Computation: Theory and Practice*, edited by P. Minev, and Y. Lin, Vol. 7, Scientific Computing and Applications, Nova Science, Huntington, NY, 2001, pp. 187–200.

C. Bailly
Associate Editor